Analysis of Silicon Channel Waveguide Thermo-Optic Switches by the Image Charge Method

Daojing Zhai, Rui Zhu, Yogesh Jaluria, and Wei Jiang

***Abstract*— Employing the "image charge" method, we theoretically study the influence of key physical parameters on the thermo-optic characteristics of a channel waveguide silicon-on-insulator (SOI) Mach–Zehnder Switch. The power consumption and spatial temperature profile of such structures are given as explicit functions of various structural, thermal, and optical parameters, offering physical insight not available in finite-element simulations. Agreement with finite-element simulations is demonstrated. The trends of switching power versus various parameters provide quantitative guide for further device optimization. This approach may also be useful for efficient modeling of an integrated optical circuit containing a large number of thermo-optic devices.**

***Index Terms*— Thermo-optic effect, switch power, heat transfer, field analogy.**

I. Introduction

SILICON is becoming an attractive material in photonic integrated circuits and optoelectronic devices due to its excellent compatibility with the well-developed CMOS technology. There has been increasing interests in optical cross-connect switches and tunable devices (e.g. filters) based on the thermo-optic effect in silicon [1]–[3]. Thermo-optic effect refers to the phenomenon that temperature variation in a structure induces a change of its refractive index, and in turn leads to a phase shift for an optical signal. Note that the understanding of the thermo-optic effect helps in the design of switches, tunable filters and other tunable silicon devices.

Mach-Zehnder interferometer (MZI, Fig. 1(a)) structures are widely used in 2×2 switches [4]–[11] because they exhibit wide spectral operation and better fabrication tolerance than ring resonators [12]. An analytical theory for the thermo-optic characteristics of SOI photonic crystal waveguide-based switches has been proposed in [13] and [14], whereas an analytic theory for the more common SOI Mach-Zehnder switch based on channel waveguides remains unclear. Fundamentally, the photonic crystal waveguide structure with an embedded silicon heater has a large lateral heat spreading length, and hence can be well-approximated by a quasi-one-dimensional (1D) model, which greatly simplify the theoretical treatment. In contrast, the seemingly simpler structure of a channel waveguide with a metal heater above is a 3D problem with no simple route to be reduced to a quasi-1D problem. Hence it is actually more challenging to be formulated into an analytic theory. Note that conformal mapping is a useful method for 2D heat conduction problems [15], but is not applicable to 3D problems. Simulations of such a structure can be computationally complex and time-consuming. Some simulations may be performed for a small number of structures. However, they are not efficient for systematically studying a large ensemble of structures in which many parameters such as the oxide depths and heater size vary over a large range. Such systematic study offers the trend of device performance with various parameters and is very useful in design and optimization, particularly for a large integrated optical circuit with many thermo-optic devices [16]. In this work, drawing inspiration from the image charge method [17] in electric field theory we develop an analytical theory for the thermo-optic characteristics of a channel waveguide SOI Mach-Zehnder switch.

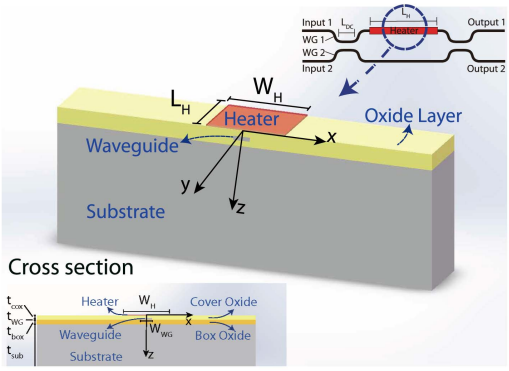

Fig. 1. Schematic configuration of a thermo-optic Mach-Zehnder switch based on channel waveguide under coordinate system. The Si waveguide is buried in oxide layer. Upper-right inset represents the overall structures of the $M-Z$ switch, where L_H is the length of heater. Low-left inset shows cross-section of the channel, where t_{cox}, t_{WG}, t_{box} and t_{sub} are the thicknesses of cover oxide, Si waveguide, box oxide and Si substrate.

Manuscript received February 10, 2019; revised February 27, 2019; accepted February 28, 2019. Date of publication March 5, 2019; date of current version April 2, 2019. This work was supported in part by the National Key R&D Program of China under Grant 2017YFA0303700 and Grant 2017YFA0303704, in part by the Natural Science Foundation of China under Grant 61775094 and Grant 41427801, in part by the Jiangsu Specially Appointed Professor Program, in part by the Fundamental Research Funds for the Central Universities under Grant 021314380072, and in part by Jiangsu Innovative/Entrepreneurial Teams. *(Corresponding author: Wei Jiang.)*

D. Zhai is with the Kuang Yaming Honors School, Nanjing University, Nanjing 210093, China.

R. Zhu and W. Jiang are with the National Laboratory of Solid State Microstructures, College of Engineering and Applied Sciences, Nanjing University, Nanjing 210093, China, also with the Key Laboratory of Intelligent Optical Sensing and Manipulation of Ministry of Education, Nanjing University, Nanjing 210093, China, and also with the Collaborative Innovation Center of Advanced Microstructures, Nanjing University, Nanjing 210093, China (e-mail: weijiang@nju.edu.cn).

Y. Jaluria is with the Department of Mechanical and Aerospace Engineering, Rutgers University, Piscataway, NJ 08854 USA.

Color versions of one or more of the figures in this letter are available online at http://ieeexplore.ieee.org.

Digital Object Identifier 10.1109/LPT.2019.2903104

The results agree well with simulations based on the finite element method (FEM). The theoretic formulas provides insightful trend as to how the key factors governing the characteristics of thermo-optic devices such as switches.

II. Analysis of SOI Channel Waveguide Thermo-Optic Structure

Figure 1 illustrates the configuration of a channel waveguide-based Mach-Zehnder switch on a SOI wafer. A heater of width W_H and length L_H is placed above the waveguide. Due to the large difference (about 100 times) in transfer coefficients between $Si\,O_2$ and Si [13], the heat transfer in $Si\,O_2$ layer plays a dominated role, and the substrate temperature change is usually very small. A number of semi-analytic methods such as the separation of varialbes and the integral method may be employed to tackle this problem approximately [18], [19]. But these generic methods do not exploit the particular geometry of the SOI channel waveguide heat conduction problem, hence it becomes fairly complicated to use these methods effectively here (e.g. resulting in slow convergence in computation). It is known that the steady-state heat transfer equation resembles the static electric field equation as both are Poisson's equation. We can utilize an electric field analogy to obtain the temperature profile. For the 3D structure, it is non-trivial to find an analytic solution of the electric field in such a structure. Here we take advantage of the large thermal conductivity difference between silicon and silicon oxide to simplify the problem, and utilize the method of image [17] in the electric field theory to find an analytic solution. The results will be verified by finite element simulation.

By such an analogy, a heat source corresponds to a charge source, the temperature corresponds to the electric potential, and the thermal conductivity corresponds to the dielectric constant. In the analogous electric structure, an electric field is induced by a finite thin sheet of charge located at the heater position (in the $z = 0$ plane). Note that in the original structure, the heat transfer process occurs mostly in the half space $z < 0$. The heat escapes from the top surface through convection and radiation is negligible (typically about $4 \sim 5$ orders of magnitude smaller than conduction in the silicon chip), which can be easily verified by using the well-established convection and radiation heat transfer formulas [18], [19]. Direct theoretical treatment of such a half space problem in $z > 0$ can be unnecessarily complicated. To facilitate the theoretical analysis, we create an image of the structure in the half space ($z < 0$) into the half space $z > 0$, and the full structure in the whole space is shown in Fig. 2(a). Now the heat transfer in the other half space is exactly same as the original structure (note that the z-component of the heat flux changes sign).

If the sheet charge is placed in an homogeneous medium, the potential drop along the z-axis due to a finite sheet of charge uniformly distributed on the x-y plane and centered at the origin is given by [17]

$$V(z)-V(0)=-\int_0^z \frac{\rho_s}{\pi\epsilon}\arctan\left(\frac{(L/2)(W/2)}{z'\sqrt{(L/2)^2+(W/2)^2+z'^2}}\right)dz' \quad (1)$$

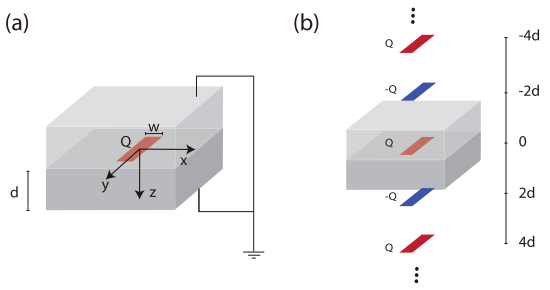

Fig. 2. Electric field analogy. (a) A finite sheet of charge is placed in the $z = 0$ plane. The top and bottom boundaries of the medium are grounded. $d = t_{cox} + t_{WG} + t_{box}$, $W = W_H$. (b) Utilize image charges to solve the problem.

where ρ_s is the charge density ($\rho_s = Q/(WL)$), ϵ is the permittivity, while W and L are the width and length of the charge sheet. By the thermal-electrical analogy, for a similar heat source of width W_H and length L_H, the temperature profile along z-axis in a semi-infinite ($z > 0$) homogeneous medium is given by substitution $W \to W_H$, $L \to L_H$, $Q \to 2P$ and $\epsilon \to \kappa$ into Eq. (1), where P is the power of the heat source, and κ is the thermal conductivity of the surrounding medium (silicon oxide here). Note the z axis points downward and $z = 0$ is assumed to be on the top surface of the oxide layer. The factor 2 is due to the replicating the original semi-infinite medium into the half-space $z < 0$ (effectively we add a source at $z = 0^-$ and convert this half space problem into a full space problem with a heat source of total power $2P$).

In the structure shown in Fig. 2(a), there are two thick silicon regions at $z > d$ and $z < -d$. In addition, there are two silicon waveguide cores. Since the cross-sectional area of the silicon waveguides are very small (typical width around 500 nm and typical height around 200 - 300 nm), their thermal effect can be neglected with minimal loss of accuracy. The two silicon substrates are more difficult to handle. Noting that the thermal conductivity of silicon is about two orders of magnitude higher than that of the silicon oxide, we may approximate silicon oxide as an electric insulator and silicon as an electric conductor by the electric analogy. By such an analogy, the bottom of the buried oxide layer can be considered as grounded by a conductor (i.e. having equal potential). For the structure in Fig. 2(a), there will be two conductors at the $z = d$ and $z = -d$ planes. Now by the electric analogy, each conductor serves as a mirror and creates an image charge of opposite sign at $z = d$ and $z = -d$, respectively. Furthermore, the image charge $-Q$ at $z = 2d$ will generate another image charge of Q at $z = -4d$ by the mirror at $z = -d$, and the image charge $-Q$ at $z = -2d$ will generate another image charge of Q at $z = 4d$ by the mirror at $z = d$, so on and so forth. The final result is an infinite series of charges of alternating signs at $z = 0, \pm 2d, \pm 4d, \ldots$, as shown in Fig. 2(b). Now the problem is converted to calculating the potential due to a series of positive/negative charges, and the effect of the conductors is effectively provided by the image charges according to the image charge method [17] (one can readily verify that this new problem satisfies the conductor's boundary condition at $z = \pm d$). The potential due to such a series of charges can be readily calculated by an infinite sum.

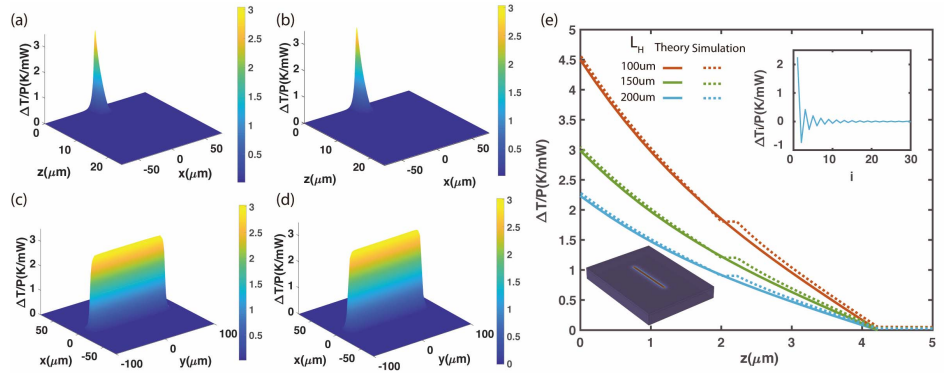

Fig. 3. Temperature profile in representative cross-sections (taking the temperature at the bottom surface of the substrate as the reference temperature); with $t_{cox} = t_{box} = 2\ \mu m$, $W_H = 4\ \mu m$, $W_{WG} = 500\ nm$, $t_{WG} = 220\ nm$, and a heating power $P = 1\ mW$. (a) FEM Simulation results in y cross-section for a device with $t_{sub} = 20\ \mu m$, $L_H = 150\ \mu m$. (b) Result in y cross-section by the image charge method. (c) FEM Simulation results in $z = 0$ plane. (d) Result in $z = 0$ plane by the image charge method. (e) Results of a device with $t_{sub} = 20\ \mu m$ and various L_H. The first 10 terms (i.e. 10 pairs of charges) are included in calculation. Upper-right inset: typical convergence characteristics of the alternating series with the number of charge pairs. Lower-left inset: overall FEM result.

Note that for each pair of charges (who are mutual images with respect to plane $z = d$), there are two integrals in form of Eq. (1) with bounds $\int_0^{z+2(i-1)d} - \int_0^{2id-z} = \int_{2id-z}^{z+2(i-1)d}$. For the analogous heat transfer problem, the solution along the z axis can be written as

$$\Delta T(z) = T(z) - T(0) = \frac{2P}{\pi \kappa W_H L_H} \sum_{i=1}^{+\infty} (-1)^{i-1} \times \int_{2(i-1)d+z}^{2id-z} \arctan\left(\frac{(L_H/2)(W_H/2)}{z' \sqrt{(L_H/2)^2 + (W_H/2)^2 + z'^2}} \right) dz', \tag{2}$$

Note that the lower and upper bounds of each integral is shifted by an amount according to the "image charge" location in the series. The integral in Eq. (2) has a fairly lengthy result,

$$\gamma_i(z; W_H, L_H) := \{ z' \arctan[\frac{(\frac{L_H}{2})(\frac{W_H}{2})}{z'\mu(z')}] - \frac{L_H}{2} \times \operatorname{arcoth}[\frac{\mu(z')}{\frac{W_H}{2}}] - \frac{W_H}{2} \operatorname{arcoth}[\frac{\mu(z')}{\frac{L_H}{2}}] \}\Big|_{2(i-1)d+z}^{2id-z}, \tag{3}$$

where $\mu(z) = \sqrt{(L_H/2)^2 + (W_H/2)^2 + z^2}$. Hence $\Delta T(z) = \frac{2P}{\pi \kappa W_H L_H} \sum_{i=1}^{+\infty} (-1)^{i-1} \gamma_i(z; W_H, L_H)$.

For temperature at arbitrary (x, y, z), direct analytic integration of "potential" from $(0, 0, 0)$ to (x, y, z) becomes difficult. Fortunately, we find it possible to first integrate in-plane to $(x, y, 0)$ then to (x, y, z), which yields

$$\Delta T(x, y, z) = \frac{2P}{\pi \kappa W_H L_H} \sum_{i=1}^{+\infty} (-1)^{i-1} \gamma_i^{(T)}(x, y, z; W_H, L_H), \tag{4}$$

where

$$\gamma_i^{(T)}(x, y, z; W_H, L_H) = \gamma^{(T)}(x, y, 0) + [\gamma_i(z; W_H - 2x, L_H - 2y) - \gamma_i(z; -W_H - 2x, L_H - 2y) - \gamma_i(z; W_H - 2x, -L_H - 2y) + \gamma_i(z; -W_H - 2x, -L_H - 2y)]/4,$$

and the in-plane integral $\gamma^{(T)}(x, y, 0) = I(x, y) - I(0, 0)$,

$$I(x, y) = \frac{1}{4} \int_{-\frac{W_H}{2}}^{\frac{W_H}{2}} \operatorname{arcsinh} \frac{|\Delta y|}{|x' - x|} \Big|_{\Delta y = -\frac{L_H}{2} - y}^{\frac{L_H}{2} - y} dx'.$$

This is readily integrated as $\int \operatorname{arcsinh} \frac{y}{x} dx = x \operatorname{arcsinh} \frac{y}{x} + y \operatorname{arcsinh} \frac{x}{y}$ (for $x > 0$ and $y > 0$).

We have conducted FEM simulation of the heat transfer and compare the simulation results with the theoretical result. The FEM simulation results for the temperature profile in the y cross-section and heater plane are plotted in Fig. 3(a)(c) for a typical structure with cover oxide and buried oxide thicknesses of $t_{cox} = t_{box} = 2\ \mu m$; a heater width of $W_H = 4\ \mu m$, length of $L_H = 150\ \mu m$; and waveguide dimensions of $W_{WG} = 500\ nm$, $t_{WG} = 220\ nm$. Note T_0 specifies the ambient temperature. As depicted in Fig. 3(a), The temperature in the silicon substrate is almost a constant and is very close to T_0 due to the very large thermal conductivity of silicon (compared to that of silicon oxide). The result based on the image charge method is shown in Fig. 3(b)(d), which agrees well with Fig. 3(a)(c). The FEM simulation results and the analytical theory results for the temperature distribution along the z-axis are compared in Fig. 3(e) for three different heater lengths. They agree well. Note that in the FEM simulation, the small silicon waveguide core creates a small constant-temperature region, but this has little impact on the overall temperature variation in the silicon oxide region. As could be expected, the (total) temperature rise in the waveguide increases as L decreases.

It should be mentioned that the infinite sum in Eq. (4) converges well. Each term in the sum represent the contribution from a "image charge pair" $(+Q/-Q)$. As n increases, the charges are farther from the silicon core and consequently their contribution to temperature in the core decreases very fast (see Fig.3(c) inset). When 10 terms are considered, the sum approaches the convergence value with an error less than 4%, and the error <3% when 20 terms taken into consideration. In practice, the results of first 10 terms works well in common case. Note that prior work [14] has shown that in SOI photonic devices, the substrate temperature rise usually contributes a very small fraction (estimated <5% here) of the total

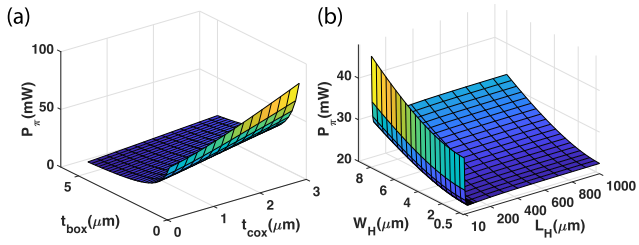

Fig. 4. Switching power trend vs. key device parameters. (a) P_π vs. t_{box} and t_{cox}, for $W_H = 4\ \mu m$ and $L_H = 100\ \mu m$. (b) P_π vs. W_H and L_H, for $t_{box} = 2\ \mu m$ and $t_{cox} = 2\ \mu m$.

temperature rise for typical heater sizes ($<500\ \mu m$) and substrate thicknesses. Therefore, the substrate effect is neglected in most cases. Note that compared to 3D FEM, this method saves memory by $\sim$1000 times, and saves time by $>500,000$ times for one point or >5000 times for 100 points (note that in many practical problems, we only need temperature at a small number of points). This method can be easily applied to many other heater shapes (e.g. L-shape, T-shape, serpentine) by decomposing them into rectangles. Detailed discussion is beyond the scope of this Letter.

III. Thermo-Optic Characteristics & Switching Power

In a Mach-Zehnder thermo-optic switch shown in Fig. 1, one can readily calculate the phase shift based on the temperature change according to $d\Phi/dy = \frac{2\pi}{\lambda}(\frac{dn}{dT})\Delta T_{core}$, where λ is the wavelength of light signal, $(dn/dT)_{Si}$ is the thermo-optic coefficient of silicon, and ΔT_{core} is the change in the temperature in the silicon core. In the bar state, the heater is turned on. After the beam from WG1 is split via the first directional coupler and then achieves a π-phase shift under the heater, the divided light beams are combined via another directional coupler and output from the bar port Output 1. On the contrary, once the heater is turned off, the light signal would output from the cross port Output 2. Utilize the principle of thermo-optic effect, we achieve an active switch function on optics devices. Note that the core is located at $z = t_{cox} + \frac{t_{WG}}{2}$, one may find the switching power of Mach-Zehnder switch needed for π phase shift with the help of Eq.(4). The P_π dependences on key parameters are obtained in Fig. 4. It can be observed in Fig. 4(a) that the value of P_π increases as the buried oxide thickness t_{box} decreases and the cover oxide thickness t_{cox} increases. Also, Fig. 4(b) indicates that P_π increases as the heater width W_H increases, and shows little variation with L_H for commonly used heater lengths ($>20\ \mu m$). Generally, changing the thicknesses of two oxide layers are more effective to modify the switching power. The switching power varies less with changing W_H.

IV. Conclusion

In conclusion, the thermo-optic characteristics of active channel waveguide SOI Mach-Zehnder Switch are investigated by the image charge method. The switching power consumption P_π and spatial temperature profile are given as explicit functions of structural, thermal, and optical parameters with no fitting parameters. The results agree well with FEM simulations. The analytic formulas and the trends of the switching power with various physical parameters offer insight into further performance optimization of SOI thermo-optic switches. This theory can also be applied to model a large-scale integrated optical circuit containing a large number of thermo-optic devices (e.g. switches, tunable filters) with channel waveguide geometry and varying heater lengths or widths. While FEM simulations for a large number of devices distributed over a *centimeter-scale* chip may demand prohibitive amount of time and memory, this theory can model them very efficiently.

References

[1] R. Soref, "The past, present, and future of silicon photonics," *IEEE J. Sel. Topics Quantum Electron.*, vol. 12, no. 6, pp. 1678–1687, Nov./Dec. 2006.
[2] B. G. Lee, A. Biberman, J. Chan, and K. Bergman, "High-performance modulators and switches for silicon photonic networks-on-chip," *IEEE J. Sel. Topics Quantum Electron.*, vol. 16, no. 1, pp. 6–22, Jan./Feb. 2010.
[3] L. Chen, E. Hall, L. Theogarajan, and J. Bowers, "Photonic switching for data center applications," *IEEE Photon. J.*, vol. 3, no. 5, pp. 834–844, Oct. 2011.
[4] U. Fischer, T. Zinke, B. Schuppert, and K. Petermann, "Singlemode optical switches based on SOI waveguides with large cross-section," *Electron. Lett.*, vol. 30, no. 5, pp. 406–408, Mar. 1994.
[5] M. W. Geis, S. J. Spector, R. C. Williamson, and T. M. Lyszczarz, "Submicrosecond submilliwatt silicon-on-insulator thermooptic switch," *IEEE Photon. Technol. Lett.*, vol. 16, no. 11, pp. 2514–2516, Nov. 2004.
[6] T. Chu, H. Yamada, S. Ishida, and Y. Arakawa, "Compact $1 \times N$ thermo-optic switches based on silicon photonic wire waveguides," *Opt. Express*, vol. 13, no. 25, pp. 10109–10114, 2005.
[7] L. Sanchez, A. Griol, S. Lechago, A. Brimont, and P. Sanchis, "Low-power operation in a silicon switch based on an asymmetric mach–zehnder interferometer," *IEEE Photon. J.*, vol. 7, no. 2, Apr. 2015, Art. no. 6900308.
[8] K. Liu, C. Zhang, S. Mu, S. Wang, and V. J. Sorger, "Two-dimensional design and analysis of trench-coupler based silicon mach-zehnder thermo-optic switch," *Opt. Express*, vol. 24, no. 14, pp. 15845–15853, 2016.
[9] S. Chen, Y. Shi, S. He, and D. Dai, "Low-loss and broadband 2×2 silicon thermo-optic mach–zehnder switch with bent directional couplers," *Opt. Lett.*, vol. 41, no. 4, pp. 836–839, 2016.
[10] R. Zhu, X. Zhou, N. Yang, L. Leng, W. Jiang, and W. Jiang, "Towards high extinction ratio in silicon thermo-optic switches—Unravelling complexity of fabrication variation," *IEEE Photon. J.*, vol. 10, no. 4, Aug. 2018, Art. no. 7905708.
[11] Y. Shoji, K. Kintaka, S. Suda, H. Kawashima, T. Hasama, and H. Ishikawa, "Low-crosstalk 2×2 thermo-optic switch with silicon wire waveguides," *Opt. Express*, vol. 18, no. 9, pp. 9071–9075, 2010.
[12] W. Bogaerts *et al.*, "Silicon microring resonators," *Laser Photon. Rev.*, vol. 6, no. 1, pp. 47–73, Jan. 2012.
[13] M. Chahal, G. K. Celler, Y. Jaluria, and W. Jiang, "Thermo-optic characteristics and switching power limit of slow-light photonic crystal structures on a silicon-on-insulator platform," *Opt. Express*, vol. 20, no. 4, pp. 4225–4231, 2012.
[14] W. Song, M. Chahal, G. K. Celler, Y. Jaluria, G. T. Reed, and W. Jiang, "The influence of substrate on SOI photonic crystal thermo-optic devices," *Opt. Express*, vol. 21, no. 4, pp. 4235–4243, 2013.
[15] A. Augustin, A. Kostka, and B. Maj, "Analytical solutions for two-dimensional heat spread in ASICs using conformal mapping techniques," in *Proc. 6th Int. Conf. Therm., Mech. Multi-Phys. Simulation Exp. Micro-Electron. Micro-Syst.*, Berlin, Germany, Apr. 2005, pp. 590–596.
[16] Y. Shen *et al.*, "Deep learning with coherent nanophotonic circuits," *Nature Photon.*, vol. 11, pp. 441–446, Jun. 2017.
[17] W. H. Hayt and J. A. Buck, *Engineering Electromagnetics*, 7th ed. Boston, MA, USA: McGraw-Hill, 2006.
[18] M. N. Ozisik, *Heat Conduction*, 2nd ed. New York, NY, USA: Wiley, 1993.
[19] Y. Jaluria and K. E. Torrance, *Computational Heat Transfer*. Washington, DC, USA: Hemisphere, 1986.